Environmental Science
Processes & Impacts

PAPER

View Article Online
View Journal | View Issue

Cite this: *Environ. Sci.: Processes Impacts*, 2017, **19**, 507

Aqueous singlet oxygen reaction kinetics of furfuryl alcohol: effect of temperature, pH, and salt content†

Elena Appiani,‡[a] Rachele Ossola,‡[a] Douglas E. Latch,[b] Paul R. Erickson*[a] and Kristopher McNeill*[a]

Received 2nd December 2016
Accepted 14th February 2017

DOI: 10.1039/c6em00646a

rsc.li/process-impacts

The rate constant for the reaction between furfuryl alcohol (FFA) and singlet oxygen ($^1O_2$) in aqueous solution was measured as a function of temperature, pH and salt content employing both steady-state photolysis (β value determination) and time-resolved singlet oxygen phosphorescence methods. The latter provided more precise and reproducible data. The reaction rate constant, $k_{rxn,FFA}$, had a relatively small temperature dependence, no pH dependence and showed a small increase in the presence of high salt concentrations (+19% with 1 M NaCl). A critical review of the available literature suggested that the widely used value of 1.2×10^8 M^{-1} s^{-1} is likely overestimated. Therefore, we recommend the use of 1.00×10^8 M^{-1} s^{-1} for reactions performed in low ionic strength aqueous solutions (freshwater) at 22 °C. Furthermore, corrections are provided that should be applied when working at higher or lower temperatures, and/or at high salt concentrations (seawater).

Environmental impact

Singlet oxygen is a short-lived oxidant formed in sunlit surface waters and is important to the fate of anthropogenic and naturally occurring organic compounds. Due to its short lifetime, the use of molecular probes to quantify its steady-state concentration are needed. Furfuryl alcohol has become the most widely used probe molecule for singlet oxygen studies. This work greatly improves the utility of furfuryl alcohol as a singlet oxygen probe by assessing the reaction rate constant under a wide variety of environmentally relevant conditions.

Introduction

Singlet oxygen ($^1O_2$, O_2 ($^1\Delta_g$)), the first electronic excited state of dioxygen, is widely studied due to its importance in both biological and environmental systems. In the context of aquatic photochemistry, $^1O_2$ was first recognized as a potentially important species in sunlit surface waters by Zepp in 1977.[1] Singlet oxygen is a selective electrophile, reacting primarily with anilines, electron-rich phenols, S-containing compounds, furans and other electron-rich heterocycles.[2–4] It is worth noting that five naturally occurring amino acids (histidine, tryptophan, tyrosine, methionine, cysteine) fall into these categories.[5–7] Singlet oxygen has been shown to be the main oxidant for histidine photodegradation in natural waters, accounting for essentially 100% of its sunlight-mediated degradation.[5] Singlet oxygen is also involved in the environmental degradation of proteins, viruses and biomolecules, making it an important species in carbon cycling.[6–12] In addition, $^1O_2$ contributes to the photodegradation of well-known micro-pollutants such as the fungicide propiconazole[13] and antibiotics belonging to the sulfonamide group.[14] It has also been found to be the primary reactive species responsible for cimetidine[15] and bacitracin A[16] photochemical decomposition.

From Zepp's initial report of $^1O_2$ in surface waters onward, the study of $^1O_2$ in environmental systems has relied heavily on the use of $^1O_2$-reactive molecular probe molecules. In 1984, Haag *et al.* proposed the use of furfuryl alcohol (FFA) and since that time it has become the standard probe molecule for $^1O_2$.[18] There are several reasons for FFA's ascendancy. Nardello *et al.* outlined several criteria for an ideal $^1O_2$ probe:[17] (1) it must be water soluble; (2) it must react selectively and with high rate constants with $^1O_2$; (3) it should not absorb light at the working wavelength(s); (4) it should not quench $^1O_2$ or sensitizer triplets physically; (5) it must form stable products; and, (6) it should be indefinitely stable under dark conditions. FFA meets all of these requirements. In addition, it is commercially available, inexpensive, and has excellent chromatographic properties.

Critical to its use as a probe molecule is FFA's bimolecular reaction rate constant with $^1O_2$, $k_{rxn,FFA}$. Most workers in the

[a]Institute of Biogeochemistry and Pollutant Dynamics (IBP), Department of Environmental Systems Science, ETH Zurich, 8092 Zurich, Switzerland. E-mail: paul.erickson@env.ethz.ch; kris.mcneill@env.ethz.ch

[b]Department of Chemistry, Seattle University, Seattle, Washington 98122, USA

† Electronic supplementary information (ESI) available. See DOI: 10.1039/c6em00646a

‡ These authors contributed equally to this work and are listed alphabetically.

field of environmental chemistry use the value reported by Haag *et al.* in 1984 of 1.2×10^8 M^{-1} s^{-1},[18] which was determined indirectly through O_2 consumption in photoirradiated aqueous solutions containing Rose Bengal. Our group and a few others have used 0.83×10^8 M^{-1} s^{-1}, a value that is 30% lower, which was based on direct observation of $^1O_2$ quenching by FFA in D_2O by time-resolved phosphorescence.[15] Over the past few years, it has become clear to us that there are reasons to be suspicious of both of these values. For instance, careful reading of the initial report of Haag *et al.* reveals that they did not measure 1.2×10^8 M^{-1} s^{-1}; rather, they determined a value of 1.09×10^8 M^{-1} s^{-1} at 22 °C and averaged it with the previously reported rate constant of 1.4×10^8 M^{-1} s^{-1} measured at 37 °C by Sluyterman.[18,19] The time-resolved phosphorescence-based value that we determined was based on the assumption that FFA was not significantly consumed during the brief laser irradiation period, which we now believe to likely be incorrect. The shortcomings of these previous measurements will be discussed in more detail below, but suffice it to say that there was good motivation to re-evaluate the FFA-$^1O_2$ rate constant.

In addition to re-measuring the rate constant for FFA and $^1O_2$, we felt it was also important to undertake an evaluation of the effects of temperature, pH and salt concentration on $k_{rxn,FFA}$. It is valuable to understand these effects not only because of the natural variability of surface waters (*e.g.*, freshwater *vs.* seawater), but also because of the fact that mechanistic or *in situ* investigations may require, for example, a wide range of temperatures and pH values.

In the present study, we used two different methods for the determination of the rate constant of $^1O_2$ and FFA. In the first method, we followed the initial rate of FFA consumption in the presence of $^1O_2$ at various FFA concentrations. The initial rate saturates at sufficiently high FFA concentrations and the half-saturation concentration of FFA (the beta value, β) can be directly related to $k_{rxn,FFA}$. This is similar to the method of Haag *et al.*, but following FFA instead of O_2 consumption. We reasoned that this would be a more direct measure of the bimolecular reaction rate constant, as there might be other reactions that consume O_2 besides that of FFA with $^1O_2$. In the second method, we followed the kinetics of $^1O_2$ relaxation in the presence of increasing concentrations of FFA by time-resolved phosphorescence laser spectroscopy. These experiments were performed in H_2O, which was deemed better than previous measurements in D_2O, as it is unknown whether there is a solvent isotope effect on $k_{rxn,FFA}$. This latter method proved to be highly precise and reproducible and was therefore used further to determine the temperature, pH, and salt concentration dependence of $k_{rxn,FFA}$.

Materials and methods

Materials

Perinaphthenone (PN), sodium bromide, guanidinium chloride, lithium chloride and sodium phosphate dibasic were purchased from Sigma Aldrich. Furfuryl alcohol (FFA) was obtained from Merck, and purified by distillation prior to use. Sodium bicarbonate, sodium chloride and magnesium dichloride hexahydrate were also purchased from Merck. Potassium dihydrogen phosphate, magnesium sulfate heptahydrate, calcium dichloride dehydrate, sodium perchlorate monohydrate and potassium chloride were from Fluka. D_2O was obtained from Armar. All solvents used for the analysis were of HPLC grade. All aqueous solutions were prepared in ultrapure water (resistivity > 18 MΩ, Barnstead Nanopure Diamond System). N_2 (99.999%) and O_2 (99.9995%) were purchased from CarbaGas.

Steady-state photolysis experiments

Theoretical background. In line with earlier studies,[18,19] $k_{rxn,FFA}$ was measured using the method of the initial rates (or β value determination). One can write the rate of FFA consumption as follows:

$$-\mathrm{d[FFA]}/\mathrm{d}t = k_{rxn,FFA}[^1O_2]_{ss}[\mathrm{FFA}], \quad (1)$$

where $[^1O_2]_{ss}$ is the $^1O_2$ steady-state concentration and $k_{rxn,FFA}$ [M^{-1} s^{-1}] is the second-order reaction rate constant of FFA with singlet oxygen. Assuming that $^1O_2$ is a reactive intermediate and that its concentration is low and constant over time, it is possible to apply the steady-state approximation and derive an expression for $[^1O_2]_{ss}$.[20]

$$\left[^1O_2\right]_{ss} = \frac{R_f}{k_d^\Delta + k_{rxn,FFA}[\mathrm{FFA}]} \quad (2)$$

where R_f [M s^{-1}] is the $^1O_2$ formation rate and k_d^Δ [s^{-1}] is the deactivation rate constant (in water $k_d^\Delta = (2.5 \pm 0.1) \times 10^5$ s^{-1}).[21] In the present work, we determined a slightly faster rate constant of $k_d^\Delta = (2.76 \pm 0.02) \times 10^5$ s^{-1} at 20 °C (see ESI†). By substituting eqn (2) into eqn (1) and substituting $\beta = k_d^\Delta / k_{rxn,FFA}$, one obtains eqn (3), here expressed in terms of initial FFA concentration and initial degradation rate.

$$-\left(\frac{\mathrm{d[FFA]}}{\mathrm{d}t}\right)_0 = R_0^{FFA} = \frac{R_f[\mathrm{FFA}]_0}{\beta + [\mathrm{FFA}]_0} \quad (3)$$

Fig. 1 shows a plot of R_0^{FFA} *vs.* $[\mathrm{FFA}]_0$. The curve is an example of saturation kinetics, and as such is characterized by two parameters: R_f and β. The formation rate (R_f, [M s^{-1}]) represents the asymptote of the curve, and is thus the maximum FFA

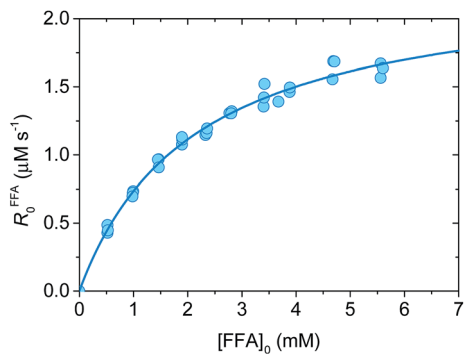

Fig. 1 Plot of R_0^{FFA} *vs.* $[FFA]_0$ at pH 8. The circles are the experimental points (in triplicate), while the line represents the non-linear curve fit. For the curve shown $R_f = (2.31 \pm 0.06)$ μM s^{-1} and $\beta = (2.1 \pm 0.1)$ mM, yielding $k_{rxn,FFA} = (1.17 \pm 0.07) \times 10^8$ M^{-1} s^{-1}.

degradation rate ($R_f = R_0^{FFA} = R_{0,max}^{FFA}$ when $[FFA]_0 \gg \beta$). The half-saturation constant β [M] corresponds to the FFA concentration that gives $R_0^{FFA} = 1/2 \times R_f$. β is the parameter of interest in this study, since it can be used to derive $k_{rxn,FFA}$ *via* eqn (4).

$$k_{rxn,FFA} = \frac{k_d^{\Delta}}{\beta} \quad (4)$$

Experimental design. Solutions of FFA (0.5–6 mM FFA + 10 mM NaCl, 10 mL) were added to a custom-made, borosilicate glass jacketed reactor with an open top. The reactor jacket was connected to a thermostated water circulator to keep the temperature constant within 0.1 °C during each experiment. A medium-pressure mercury lamp (Oriel Apex Illuminator, Newport) with a 365 nm bandpass filter was used as the light source. Prior to irradiation, solutions were saturated with O_2, equilibrated to the desired temperature, and pH-adjusted by addition of HCl or NaOH. Once the pH and the temperature were stable, perinaphthenone (PN) was added to a final concentration of 10 μM and the irradiation was started. During the reaction, the pH was kept constant by addition of KOH through an automatic titrator, and the temperature monitored. Samples were collected every 30 s and analyzed by reverse-phase HPLC (Waters, reverse phase C18 column; eluent: 15% acetonitrile, 85% pH 5 acetate buffer). The slope of [FFA] *vs.* time provided the initial reaction rate, R_0^{FFA}. The initial rates data, R_0^{FFA} *vs.* $[FFA]_0$, were fit to eqn (3) to yield R_f and β. The experiments were performed in triplicate at each pH value (4, 5, 6, 8, and 10; $T = 26$ °C) and temperature (6, 10, 14, 26 and 47 °C; pH 8).

Time-resolved singlet oxygen phosphorescence experiments

Theoretical background. Time-resolved singlet oxygen phosphorescence is the most direct and specific method for monitoring $^1O_2$.[22–25] Eqn (5)–(8) show a summary of singlet oxygen deactivation processes in the presence of a quencher Q. As pointed out in the introduction, the lifetime of singlet oxygen in aqueous solution is relatively short (3.6 μs, see ESI†), being controlled by its fast deactivation by the solvent (k_d^{Δ}, eqn (5)). However, a very small fraction of the $^1O_2$ population still undergoes radiative decay, emitting photons at 1270 nm. This weak phosphorescence can be recorded in a time-resolved manner and used to extract information about the system dynamics.

$$^1O_2 \xrightarrow{k_d^{\Delta}} O_2 \quad (5)$$

$$^1O_2 \xrightarrow{k_R^{\Delta}} O_2 + h\nu_{1270} \quad (6)$$

$$^1O_2 + Q \xrightarrow{k_{rxn,Q}} Q(O_2) \quad (7)$$

$$^1O_2 + Q \xrightarrow{k_{phys,Q}} O_2 + Q \quad (8)$$

By integration of the kinetic rate law, it is possible to demonstrate that the $^1O_2$ concentration will follow a growth and decay profile as described by eqn (9).[27]

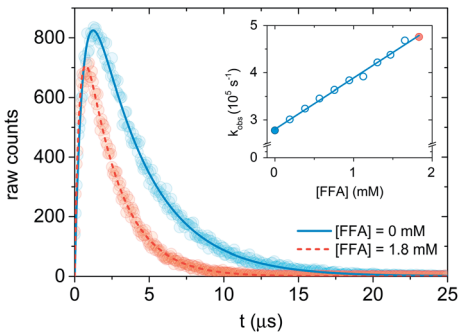

Fig. 2 Singlet oxygen formation and decay profiles in the presence of 0 mM (blue) and 1.8 mM (red) FFA recorded with 75 μM PN in MilliQ water for 10 s. The circles represent the experimental points, and the lines are the curve fits performed with Origin (eqn (12)). For data analysis, decay portions were fit to a monoexponential function (eqn (10)). The insert is the Stern–Volmer plot obtained with the experimental data. The points associated with the signal in the main plot are highlighted in blue and red.

$$\left[^1O_2\right](t) = \left[^3Sens\right]_0 \frac{k_T}{k_\Delta - k_T}\left(e^{-k_T t} - e^{-k_\Delta t}\right), \quad (9)$$

where $[^3Sens]_0$ is the concentration of sensitizer in the triplet state, k_T and k_Δ are the triplet sensitizer and singlet oxygen total deactivation rate constants, respectively. The phosphorescence signal S is directly proportional to both $[^1O_2]$ and the singlet oxygen radiative decay rate constant, k_R^{Δ} (see eqn (6)). Therefore,

$$S(t) = A_0 \frac{\tau_\Delta}{\tau_\Delta - \tau_T}\left(e^{-t/\tau_\Delta} - e^{-t/\tau_T}\right) \quad (10)$$

where A_0 is a preexponential factor proportional to k_R^{Δ} and the $^1O_2$ formation quantum yield (Φ_Δ), and $\tau_i = 1/k_i$ are the singlet oxygen (i = Δ) and the triplet (i = T) lifetimes. Fig. 2 shows examples of signals collected using the experimental setup, with PN as photosensitizer. As elucidated from the above expression (10), when $\tau_\Delta > \tau_T$ the signal grows with the triplet lifetime and decays with the $^1O_2$ lifetime. This is the case when performing experiments in water ($\tau_\Delta \approx 4$ μs) with perinaphthenone ($\tau_T \approx 0.40$ μs in oxygen saturated solutions).[28] Thus, the decay portion of the phosphorescence signal provides information about the $^1O_2$ deactivation/reaction kinetics. The decay constant, $k_\Delta = 1/\tau_\Delta$, is the sum of the various relaxation processes (eqn (5)–(8)). In the particular case of FFA reaction with singlet oxygen, only unimolecular relaxation (k_d^{Δ}, eqn (5)) and reactive-quenching ($k_{rxn,FFA}[FFA]$, eqn (7)) are kinetically important, leading to eqn (11).[29,30]

$$k_\Delta = k_d^{\Delta} + k_{rxn,FFA}[FFA] \quad (11)$$

Therefore, a plot of k_Δ *vs.* [FFA] provides $k_{rxn,FFA}$ from the slope of the regression line (Stern–Volmer plot, insert in Fig. 2),[31] while the intercept yields the solvent deactivation rate constant k_d^{Δ} (experimental values in the ESI†).

Experimental setup

Time-resolved $^1O_2$ phosphorescence experiments. The experimental setup used for $^1O_2$ phosphorescence measurements was

based on a previously published design.[22] For our experiment, excitation pulses were generated by converting the primary 795 nm output of a regeneratively amplified laser (Solstice, Spectra-Physics, Darmstadt, Germany, pulse width < 100 fs, 1 kHz repetition rate) with a TOPAS optical parametric amplifier (Light Conversion, Vilnius, Lithuania) to 365 nm. A cuvette containing the sample solution was housed in a cuvette holder (Thor labs CVH100) with an integrated lens/fiber optic mount. Samples were excited with a collimated beam (spot size approx. 7 mm) set to a power of 50–70 mW. Singlet oxygen phosphorescence was monitored 90° to the excitation, and the emitted photons were first passed through a 1270 ± 5 nm bandpass filter, and collected with a lens focused onto a 1 mm i.d. optical fiber which terminates into a fiber mount attached to the window of a near-IR PMT (Hamamatsu, model H10330-45). The PMT output was sent to a preamplifier (PAM 103-P PicoQuant) and then on to a multichannel scaler (TimeHarp 260Nano, PicoQuant) for integrated photon counting. Singlet oxygen phosphorescence was collected in one of two ways. First, photon counts were integrated until approximately 600 counts were reached at the signal maximum (see Fig. 2 for an indication of the relative signal to noise achieved at 600 counts), after which the measurements were manually stopped. Second, photon counts were integrated for 10 s. Both methods provided adequate signal for reliable data fitting, and no significant differences could be seen between them. Transient data were exported to Origin for fitting and analysis.

Temperature variation experiments. A 1-cm pathlength flow-through cuvette was connected *via* Tygon tubing to a three-necked flask (250 mL) containing a solution of PN (200 mL, 75 μM PN, pH 6.8 phosphate-buffered, $I = 10$ mM corrected with NaCl). The flask, which acted as a reservoir, was placed in a stirred, temperature-controlled water bath. A peristaltic pump ensured good mixing and continuous circulation through the system. The solution was continuously circulated from the reservoir to the cuvette, and then back to the reservoir at a flow rate of approximately 2.5 mL s^{-1}. The PN solution was first equilibrated at the desired temperature, then the reservoir was purged with O_2 for approx. 5 min. An aliquot of FFA stock (400 μL, 0.1 M FFA in water) was added to the PN solution, and after 3 min of equilibration, a sample (150 μL) was removed for HPLC analysis to determine the actual FFA concentration. The FFA addition and data collection procedure was repeated 10 times, until a total FFA stock volume of 4 mL (10 × 400 μL) was added. Data were collected at seven different temperatures: 5, 10, 25, 30, 35, 40, and 45 °C.

pH effect and salt effect (concentration and type) experiments. The measurements were performed using a flow-to-waste setup. This experimental arrangement is identical to the flow-through setup except that the solution in the cuvette is flushed to a waste beaker during irradiation to avoid buildup of degradation products. A 1-cm flow-through cuvette was connected *via* Tygon tubing to a reservoir filled with PN solution (*ca.* 500 mL, 75 μM). For each pH variation experiment, the pH was adjusted to the desired value with NaOH 1 M or HCl 1 M. In NaCl concentration experiments, PN solutions were prepared in pH 6.8 phosphate buffer (10 mM), and the salt concentration was increased by addition of NaCl. Similarly, salt effect experiments were performed in pH 6.8 phosphate-buffered PN solutions at 2 M total salt concentration. For each experiment, the solution was stirred, purged with O_2, and circulated in the system for 5 min prior to analysis using a peristaltic pump. FFA (neat, 5 μL) was added to the solution, and after 2 min of equilibration, an aliquot (150 μL) was withdrawn for HPLC analysis. The FFA addition and data collection procedure was repeated 10 times, until a total FFA stock volume of 50 μL (10 × 5 μL) was added. The FFA concentration was later determined by HPLC analysis. This experiment was repeated at ten pH values, from 3 to 12, and at 6 different NaCl concentrations in the interval 0.01–1 M. The salt effect was tested on 2 M solutions of NaCl, NaBr, NaI, $NaClO_4$, LiCl, $MgCl_2$ and guanidinium chloride (GnCl). A duplicate measurement was also recorded using artificial seawater prepared according to Brujewicz.[32]

Data analysis. For all time-resolved experiments, the transient signal between 2.5 and 50 μs was fit to the mono-exponential decay function (12) (Origin 9.0).

$$S(t) = C \times e^{-t/\tau_\Delta} \quad (12)$$

Eqn (12) is a simplified form of eqn (10) that holds when only the decay portion of the singlet oxygen signal is taken into account, *i.e.*, for $t > 2.5$ μs. Prior to 2.5 μs PN is still forming $^1O_2$, thus the signal cannot be treated as a simple monoexponential decay. The reciprocal of the lifetime, $k_{obs} = 1/\tau_\Delta$, was plotted against the [FFA] determined by HPLC analysis. The bimolecular rate constant $k_{rxn,FFA}$ was obtained as the slope of the regression line (eqn (11)). Using data obtained from the temperature variation experiments, Arrhenius and Eyring plots were constructed in order to extract the activation parameters of the reaction, namely energy of activation (E_a), preexponential factor ($\ln A$), enthalpy of activation ($\Delta H^\ddagger$) and entropy of activation ($\Delta S^\ddagger$).

Results and discussion

Temperature dependence

The temperature dependence of $k_{rxn,FFA}$ was assessed over a 40 °C range (T = 5–45 °C) with both steady-state and time-resolved methods. Activation parameters determined from both Arrhenius and Eyring analyses are summarized in Table 1. As a general observation, the two methods provide comparable and consistent results. However, the time-resolved data were more reproducible and precise: lower experimental variability was observed with the time-resolved method across all of the experiments performed in this study. Therefore, the following sections will focus primarily on the time-resolved data.

Fig. 3 shows Arrhenius ($\ln k_{rxn,FFA}$ *vs.* $1/T$) and Eyring ($\ln(k_{rxn,FFA}/T)$ *vs.* $1/T$) plots used to determine the activation parameters for the time-resolved phosphorescence data. A linear regression of the former provided $E_a = (13.2 \pm 0.5)$ kJ mol^{-1} and $\ln A = 23.8 \pm 0.2$, while the Eyring analysis gave $\Delta H^\ddagger = (10.5 \pm 0.5)$ kJ mol^{-1} and $\Delta S^\ddagger = -(54 \pm 2)$ J K^{-1} mol^{-1}. The steady-state photolysis method (β determination, Fig. S2†) gave

Table 1 Summary of activation parameters obtained with steady-state (β value) and time-resolved methods

Method	T range (°C)	Arrhenius parameters		Eyring parameters		Reference
		E_a (kJ mol^{-1})	ln A	$\Delta H^{\ddagger}$ (kJ mol^{-1})	$\Delta S^{\ddagger}$ (J K^{-1} mol^{-1})	
β value FFA consumption	5–45	18 ± 2	26 ± 1	16 ± 2	−(40 ± 8)	This work
Time-resolved phosphorescence	5–45	13.2 ± 0.5	23.8 ± 0.2	10.5 ± 0.5	−(54 ± 2)	This work
β value O_2 consumption	15–45	22.7	27.8	20.2[a]	−22[a]	Gottfried and Kimel (1991)[33]
β value FFA consumption	0–23	19.9	26.9	17.6	−28.8	Gassmann (1984)[38]

[a] Converted from the Arrhenius parameters using the following relationships (T = 298 K): $E_a = \Delta H^{\ddagger} + RT$; $A = ek_BT/h \times e^{(\Delta S^{\ddagger}/R)}$.[34]

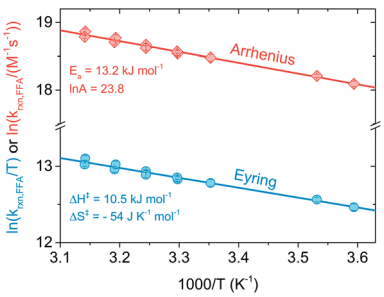

Fig. 3 Arrhenius (red diamond) and Eyring (blue circles) plots obtained from time-resolved singlet oxygen experiments performed in the temperature range 5–45 °C. Each error bar represents the standard error of the regression line of a Stern–Volmer plot.

a higher $\Delta H^{\ddagger}$ ((16 ± 3) kJ mol^{-1}) and less negative $\Delta S^{\ddagger}$ (−(40 ± 8) J K^{-1} mol^{-1}), with higher uncertainty in both values than found with time-resolved phosphorescence.

Activation parameters for the reaction of FFA with $^1O_2$ were previously determined by Gottfried and Kimel using a porphyrin sensitizer and a Clark electrode apparatus for measuring dissolved oxygen (entry 6 in Table 2).[33] Their reported values, when converted to enthalpy and entropy of activation ($E_a = \Delta H^{\ddagger} + RT$; $A = ek_BT/h \times e^{(\Delta S^{\ddagger}/R)}$),[34] are $\Delta H^{\ddagger}$ = 20.2 kJ mol^{-1} and $\Delta S^{\ddagger}$ = −22 J K^{-1} mol^{-1}, which are generally consistent with those determined here. We favor the values found in the present study as there was more precision in the individual measurements and the temperature dependence was determined over a greater temperature range (40 *vs.* 30 °C range).

It is worth noting that the enthalpy of activation determined in this study, while low, is still significantly higher than found for other furans reacting with $^1O_2$. For example, Gorman *et al.* reported $\Delta H^{\ddagger}$ of (0.0 ± 0.4) kcal mol^{-1} for the reaction of $^1O_2$ with both furan and dimethylfuran in toluene solvent.[35] Near-zero and even negative $\Delta H^{\ddagger}$ values have led to the conclusion that $^1O_2$ forms an exciplex prior to reaction. We speculate that the solvent (water) is likely the key difference giving the distinctly higher $\Delta H^{\ddagger}$ value measured here. Temperature-dependent changes in aqueous diffusion rate constants, which are due to the relatively steep viscosity–temperature relationship for water, lead to apparent activation energies of 12–20 kJ mol^{-1} (5–200 °C).[36,37]

Table 2 Chronological summary of literature reaction rate constants of FFA with singlet oxygen in water

Entry	$k_{rxn,FFA}$ (10^8 M^{-1} s^{-1})	T (°C)	$k_{rxn,FFA}$[a] (10^8 M^{-1} s^{-1})	Sensitizer[b]	Solvent	pH	Method	Reference
1	1.4	37	1.30	PF	H_2O	3–9	O_2 consumption (Warburg manometer)	Sluyterman (1961)[19]
2	1.1	9	0.79	PS-RB	H_2O	—	FFA consumption	Gassmann (1984)[38]
3	1.09 ± 0.09[c] 1.2[d]	22	1.00	RB	H_2O	7 (?)	O_2 consumption (Clark electrode)	Haag (1984)[18]
4	0.93 ± 0.15[e]	22	1.00	Hpd	15 mM NaCl, H_2O	7.4 (?)	O_2 consumption (Clark electrode)	Murasecco (1985)[51]
5	1.2	—	—	RB	H_2O	7–11.5	O_2 consumption (Clark electrode)	Scully and Hoigné (1987)[39]
6	1.4	25 (15–45)	1.06	$TPPS_4$	H_2O	6.6–7.6	O_2 consumption (Clark electrode)	Gottfried and Kimel (1991)[33]
7	0.83	23 ± 2	—	RB	D_2O	7.5	Time-resolved $^1O_2$ phosphorescence	Latch (2003)[15]
8	0.94 ± 0.01[f]	19–20 (5–45)	0.95–0.97	PN	H_2O[g]	3–12	Time-resolved $^1O_2$ phosphorescence	This work
9	1.0 ± 0.6	26 (5–45)	1.08	PN	H_2O	4–10	FFA consumption	This work

[a] Calculated with eqn (14). [b] Sensitizer abbreviations: PF = proflavine, RB = Rose Bengal, PS-RB = polystyrene-bound RB, $TPPS_4$ = *meso*-tetraphenylporphyrin tetrasulfonate, Hpd = hematoporphyrin derivative, PN = perinaphthenone. [c] Measured. [d] Reported. [e] The error is the standard deviation calculated from the two reported values. [f] The error is the standard deviation calculated from the determinations performed at the different pH values. [g] The rate constant was also determined in D_2O and no solvent isotope effect was found (k_H/k_D = 1.00 ± 0.06).

This has been interpreted as the activation energy associated with the diffusion of solutes in water.[36]

In summary, despite the relatively small enthalpy of activation, a temperature dependence on $k_{rxn,FFA}$ does exist and should be considered when performing photolysis experiments. This might be important when temperature is likely to vary or be high, for example during the course of long photolysis experiments or when high light intensities are employed. As shown in Fig. S1,† in our photoreactor, the solution temperature can increase up to 10 °C if not controlled. Using the results in Table 1 one can calculate a reaction rate enhancement of about 20% when heating the solution from 24 °C to 34 °C (from 1.04 to 1.24 $\times 10^8$ M^{-1} s^{-1}). Therefore, as a good practice, one should record the temperature trend during the experiment, and then calculate the value of $k_{rxn,FFA}$ to be used in the data analysis. The rate constant at an arbitrary temperature can be calculated using eqn (13), obtained from the linear regression of the experimental points.

$$\ln k_{rxn,FFA} = -\frac{(1.59 \pm 0.06) \times 10^3}{273.15 + T\ [°C]} + (23.82 \pm 0.21) \quad (13)$$

In the range of common laboratory and photoreactor temperatures (T = 20–40 °C), it is perfectly adequate (<0.6% error) to use the simple linear eqn (14).

$$k_{rxn,FFA} = (1.00 \pm 0.04) \times 10^8\ M^{-1}\ s^{-1} + [(2.1 \pm 0.3) \times 10^6\ M^{-1}\ s^{-1}\ °C^{-1}] \times (T - 22\ °C);\quad 20 < T < 40\ °C \quad (14)$$

This equation gives a nice rule-of-thumb that $k_{rxn,FFA}$ is 1.00 $\times 10^8$ M^{-1} s^{-1} at 22 °C and changes 2% for every degree Celsius.

pH dependence

The rate constant $k_{rxn,FFA}$ was also studied as function of pH in the range of 3–12 using both steady-state and time-resolved methods.

Our measurements are summarized in Fig. 4 and S3.† Data from the time-resolved phosphorescence method showed no pH dependence from pH 3 to 12, giving $k^{avg}_{rxn,FFA} = (9.4 \pm 0.1) \times 10^7$ M^{-1} s^{-1} (T = 19–20 °C) (Fig. 4). Measurements made between pH 4 and 10 by the steady-state method show qualitatively the same results, albeit with a much larger (*ca.* +20%) variation in the measured rate constants (Fig. S3†). The absence of a pH dependence fits the fact that neither $^1O_2$ nor FFA have pK_a values in this range. Variations in $^1O_2$ reaction rate constants that depend on pH are usually associated with a change in protonation state of the substrate. For example, rate constants for phenols are typically 2 orders of magnitude smaller than those of phenolates.[2,39,40] Histidine and histamine also have speciation-dependent reaction rate constants.[41]

The absence of a pH dependence is also in agreement with previous literature findings. Sluyterman (entry 1 in Table 2) reported a constant oxygenation rate constant for furfuryl alcohol in the pH range 3–9.[19] Similarly, Scully and Hoigné (entry 5 in Table 2) observed constant $k_{rxn,FFA}$ values at pH 7, 10 and 11.5.[39] By contrast, Gottfried and Kimel (entry 6 in Table 2) measured a 60% increase in the reaction rate constant when lowering the pH from 7.6 to 6.6. In light of the results reported here, we believe that the Gottfried and Kimel result is simply the outlier of the group, and that there is no pH dependence in $k_{rxn,FFA}$.

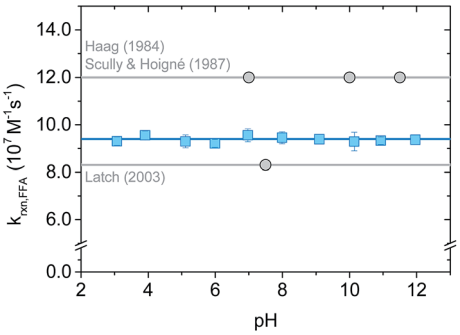

Fig. 4 pH dependence on $k_{rxn,FFA}$ studied with time-resolved singlet oxygen phosphorescence at 19–20 °C (lab temperature). The error bars indicate the standard deviation of the linear regression performed on the Stern–Volmer plot for each experiment. The blue solid line is the average value across the whole pH range; the grey lines show Haag[18] (most used) and Latch[15] (most recent) values.

Dependence on salt content

Salt concentration dependence was assessed with time-resolved $^1O_2$ phosphorescence using NaCl solutions in the ionic strength range I = 0.01–1 M. This range includes all major natural water types, from surface waters (I = 1–5 mM) to ground water (I = 10–20 mM) and seawater (I = 670 mM).[42,43] Even though the chemical nature of the ionic components can vary greatly, we focused on sodium chloride because of its abundance in a typical high-salinity environment. In a representative seawater sample (salinity 3.5%) Cl^- represents 95% of the total anions content, while Na^+ accounts for 86% of the total cations (by mole percent).[44,45]

As reported in Fig. 5, $k_{rxn,FFA}$ increases slightly with [NaCl], corresponding to a reaction rate constant enhancement of +13.4% for artificial seawater (I = 0.67 M) and +19% obtained with 1 M NaCl (I = 1.0 M). We explored two possible explanations for this increase. The first is that the ionic strength of the medium might influence the kinetics. The second is that there

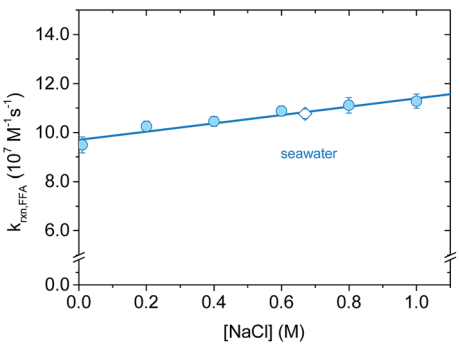

Fig. 5 Salt concentration dependence on $k_{rxn,FFA}$ determined *via* time-resolved singlet oxygen phosphorescence. The error bar represents the error of the regression line of a Stern–Volmer plot. The empty diamond is the measured value for artificial seawater. All measurements are performed at 19.5–20.5 °C (lab temperature).

Table 3 Summary of $k_{rxn,FFA}$ determined in 2 M aqueous solutions at 20 °C (lab temperature) *via* time-resolved singlet oxygen phosphorescence. The ratio $k^{salt}_{rxn,FFA}/k^{buffer}_{rxn,FFA}$ was calculated using $k_{rxn,FFA}$ measured in a 10 mM-buffered solution in the same experimental conditions ($k^{buffer}_{rxn,FFA} = (9.5 \pm 0.3) \times 10^7$ M^{-1} s^{-1}). NaI was not measured as iodide suppressed singlet oxygen production. Abbreviation: GnCl = guanidinium chloride

Salt (2 M)	$k_{rxn,FFA}$ (10^8 M^{-1} s^{-1})	$k^{salt}_{rxn,FFA}/k^{buffer}_{rxn,FFA}$	r_{cation} (pm)	r_{anion} (pm)
NaCl	1.27 ± 0.05	1.34	113[a]	167[a]
NaBr	1.28 ± 0.04	1.35	113[a]	182[a]
$NaClO_4$	1.41 ± 0.04	1.49	113[a]	226[a]
$MgCl_2$	1.1 ± 0.1	1.18	86[a]	167[a]
LiCl	1.05 ± 0.02	1.11	90[a]	167[a]
GnCl	1.02 ± 0.02	1.07	210[b]	167[a]

Reference: [a] crystal radius from Shannon.[49] [b] Calculated ionic radius from Marcus.[50]

is a salt effect similar to what has been observed for Diels–Alder reactions, which have been interpreted in terms of the hydrophobic effect.[46,47] Both of these hypotheses are testable by examining the influence of different salt compositions on the kinetics. In the first case, the kinetics should be the same for two solutions of the same ionic strength regardless of the identity of the ions involved. In the second case, the reaction should be accelerated by "salting out" ions (*e.g.*, LiCl) and decelerated by "salting in" ions (*e.g.* guanidinium chloride, GnCl), as proposed by Breslow.[46] This is the result of water–ion interactions: small, hard ions strongly bind to water, increasing the cavitation energy and therefore favoring aggregate formation between hydrophobic molecules (*i.e.*, formation of activated complexes). On the other hand, big, soft ions loosely interact with water, decreasing the cavitation energy. It has also been suggested that "salting-in" ions disrupt hydrophobic aggregation by enhancing the water solubility of organic molecules through direct interactions.[48]

Table 3 lists rate constants determined in the presence of various ions (at 2 M), and clearly demonstrates that neither of the above explanations is satisfactory. The rate constants change with different salt compositions, arguing against a simple ionic strength effect. Furthermore, the rate constants do not follow the order predicted by the hydrophobic effect hypothesis. For example, LiCl and GnCl are expected to be opposite end members, but instead show almost identical rate constants. We noted that $k_{rxn,FFA}$ increases with the anion radius, but shows a less defined trend with respect to the cation size.

Whatever the origin of the salt effect, for aquatic systems where sodium and chloride ions are dominant, it is important to note that there is an empirical linear relationship between molar concentration of NaCl and the rate constant at 20 °C (eqn (15)).

$$k^{20\ °C}_{rxn,FFA} = (9.7 \pm 0.1) \times 10^7\ M^{-1}\ s^{-1} + (1.7 \pm 0.2) \times 10^7\ M^{-2}\ s^{-1} \times [NaCl] \quad (15)$$

Comparison with previous studies

Table 2 summarizes the available literature on $^1O_2$ reaction rate constants with FFA in water. Note that for entry 3, both the widely used value of 1.2×10^8 M^{-1} s^{-1} is given, as well as the value actually measured by Haag *et al.* of $(1.09 \pm 0.09) \times 10^8$ M^{-1} s^{-1}. The latter value was calculated from the reported β value of $(2.3 \pm 0.2) \times 10^{-3}$ M, using eqn (4), while the former value was arrived at by Haag *et al.* by averaging the measured value (at 22 °C) with the previously measured value of Sluyterman (at 37 °C) (entry 1).

In general, the most common experimental technique employed until the 1990s consists of measuring the loss of ground state oxygen under pseudo first-order conditions (*i.e.*, high FFA concentrations) and then relating it to the loss of FFA assuming a 1 : 1 stoichiometric ratio. This has been done with both pressure (entry 1) and amperometric measurements (entries 3–6). Once the ground state oxygen depletion kinetics are known, it is possible to calculate $k_{rxn,FFA}$ using the β value method. The only time-resolved determination that we are aware of was performed in 2003 (entry 7). However, due to the poor response time of the available Ge-based detector, the measurement could only be performed in D_2O, where the singlet oxygen lifetime is 14 times longer than in H_2O.[26]

As far as the values are concerned, O_2 consumption-based rate constants are generally higher than what was measured in the current work. For example, Sluyterman obtained $k_{rxn,FFA} = 1.4 \times 10^8$ M^{-1} s^{-1}, while on the basis of eqn (14) one would expect $k_{rxn} = 1.30 \times 10^8$ M^{-1} s^{-1} at 37 °C. Similarly, Haag found $k_{rxn,FFA} = 1.09 \times 10^8$ M^{-1} s^{-1} at 22 °C, while we would predict it to be 9% lower. A general difference between the previous studies and ours is the choice of the sensitizer. While in the past Rose Bengal (RB) was the most commonly employed sensitizer, we decided to use perinaphthenone (PN) instead, the main reason being the pH-dependent sensitization properties of RB.[52] PN is a convenient sensitizer to use because of its UV-A absorption (λ_{max} = 365 nm), pH independent speciation and high singlet oxygen quantum yields in a variety of solvents (*i.e.*, $\Phi_\Delta = 0.95$ in water).[53–56] Indeed, because of these features PN is acknowledged as a reference compound for (photochemically generated) singlet oxygen quantum yield determinations.[54] As a further point, the very low triplet energy of PN helps to ensure that no processes other than singlet oxygen production take place from oxygen quenching of PN triplet excited state, whereas for other sensitizers oxygen quenching can also generate superoxide anions (as a result of electron transfer).[57–64]

The use of RB as a sensitizer might be problematic with respect to unwanted side reactions. Though not conclusive,

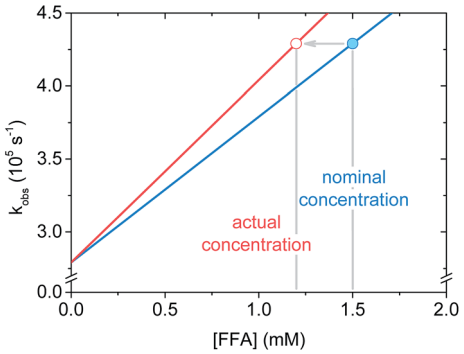

Fig. 6 Schematic graph showing the effect of furfuryl alcohol degradation on the apparent slope of the fitted line (*i.e.* the rate constant) in a Stern–Volmer plot.

several literature sources point toward the non-innocent role of a superoxide radical anion pathway in oxygen quenching of RB triplets. For instance, Srinivasan *et al.*[59] used superoxide dismutase to detect $O_2^{-\bullet}$ generated during constant steady-state irradiation of aqueous RB solution, obtaining a yield as high as 23% for superoxide radical anion formation. A similar result was observed by Lee and Rodgers, who used benzoquinone to trap $O_2^{-\bullet}$ generated upon laser flash photolysis of RB solutions ($\Phi_{O_2^{-\bullet}} = 0.20$).[60] However, Lambert and Kochevar recently questioned these findings,[65] providing experimental evidence of the inefficiency of superoxide radical anion formation in aqueous environments ($\Phi_{O_2^{-\bullet}} < 0.01$). Regardless of the mechanism, photobleaching is commonly observed for RB and other dyes. It has been shown that in the presence of oxygen and low concentration of dye ([dye] < 10 μM), sensitizer degradation follows first order kinetics, with the rate determining step being the attack of ground state oxygen on the excited triplet state (D–O mechanism).[66] Thus, several pieces of evidence suggest that RB sensitized photolysis experiments can be biased by other oxygen-consuming processes.

Regarding the $k_{rxn,FFA}$ value reported by Latch (entry 7), a reanalysis of the data revealed that the experimental design may have led to an artificially low $k_{rxn,FFA}$ value. In their experiment, they measured $k_{rxn,FFA}$ by additive spiking of an FFA stock into a single sensitizer solution which was repeatedly irradiated. In some instances this is a reasonable method, however one must consider that FFA may be consumed to a significant extent during the measurement. For slow reactions, or short irradiation times, the change in quencher concentration will be small, and may be neglected. We now make the case that FFA consumption should have been taken into account in the previous $k_{rxn,FFA}$ determination experiments. With the sensitizer concentration and laser power levels employed in the present work, about 10% of the starting FFA was consumed in a roughly 4 mL sample during the 6–10 s of signal acquisition. Fig. 6 shows that when FFA consumption is taken into account, the regression line based on the "spiked" FFA concentrations is less steep, resulting in artificially low quenching rate constants. To illustrate, for the same $[FFA]_0$ and k_{obs} values, $k_{rxn,FFA}$ increases from 8.3 to 9.7×10^7 M^{-1} s^{-1} when adjusting from 0% to 20% loss of FFA starting concentration. We think that this might explain the discrepancy between the Latch value and the one reported here.

Conclusions

The reaction rate constant for the reaction of furfuryl alcohol with singlet oxygen in water was investigated as a function of temperature, pH, and salt content using both steady-state (β value) and time-resolved methods. Temperature was the main factor influencing $k_{rxn,FFA}$, while the reaction was shown to be pH independent. A small increase in $k_{rxn,FFA}$ was observed at relatively high ionic strengths, using both NaCl and artificial seawater. In low ionic strength solutions (below 50–100 mM) the effect was negligible. In measuring k_{rxn}, time-resolved singlet oxygen phosphorescence was shown to be a superior method compared to the classical one based on β value determination due to its higher precision and reproducibility.

We discourage the use of the well-known 1.2×10^8 M^{-1} s^{-1} value of Haag *et al.*, both because it may be an overestimate due to Rose Bengal-induced side reactions and because the actual value measured in that study was 1.09×10^8 M^{-1} s^{-1}. This implies that the past values are most likely underestimated by 10–20%, depending on the solution temperature and ionic strength, as well as the assumptions in the calculation of $[^1O_2]_{ss}$ (*i.e.*, whether FFA quenching is considered or not; more details in the ESI†). Likewise, the use of the 8.3×10^7 M^{-1} s^{-1} value reported by Latch *et al.* should be discontinued due to experimental conditions that likely led to the underreporting of the true reactivity of FFA with $^1O_2$.

For future studies using FFA as a $^1O_2$ probe molecule, we recommend the following:

(1) Monitor the temperature of the sample during the photolysis experiment;

(2) Use the temperature-adjusted $k_{rxn,FFA}$ value (see eqn (13) and (14));

(3) Apply a salt content correction if working at elevated salt concentrations (*e.g.* in seawater; see eqn (15)).

Acknowledgements

This work was financially supported by a grant from the Swiss National Science Foundation (Project numbers CRSI22_127568). We thank Annika Linkhorst and Prof. Charles Sharpless (Univ. of Mary Washington) for conducting preliminary experiments and helpful discussions.

References

1 R. G. Zepp, N. L. Wolfe, G. L. Baughman and R. C. Hollis, *Nature*, 1977, **267**(5610), 421–423.
2 R. P. Schwarzenbach, P. M. Gschwend and D. M. Imboden, in *Environmental Organic Chemistry*, John Wiley & Sons, Inc., 2002, pp. 655–686.
3 E. L. Clennan and A. Pace, *Tetrahedron*, 2005, **61**(28), 6665–6691.

4 H. H. Wasserman, *Ann. N. Y. Acad. Sci.*, 1970, **171**(1), 108–120.
5 A. L. Boreen, B. L. Edhlund, J. B. Cotner and K. McNeill, *Environ. Sci. Technol.*, 2008, **42**(15), 5492–5498.
6 R. A. Lundeen, E. M.-L. Janssen, C. Chu and K. McNeill, *Chimia*, 2014, **68**(11), 812–817.
7 M. J. Davies, *Photochem. Photobiol. Sci.*, 2004, **3**(1), 17–25.
8 T. Kohn, M. Grandbois, K. McNeill and K. L. Nelson, *Environ. Sci. Technol.*, 2007, **41**(13), 4626–4632.
9 K. Rule Wigginton, L. Menin, J. P. Montoya and T. Kohn, *Environ. Sci. Technol.*, 2010, **44**(14), 5437–5443.
10 T. Sigstam, G. Gannon, M. Cascella, B. M. Pecson, K. R. Wigginton and T. Kohn, *Appl. Environ. Microbiol.*, 2013, **79**(11), 3455–3467.
11 G. Bentivenga, C. Bonini, M. D'Auria and A. J. De Bona, *Photochem. Photobiol.*, 1999, **128**(1–3), 139–143.
12 C. Bonini, M. D'Auria, G. Mauriello, D. Viggiano and F. J. Zimbardi, *Photochem. Photobiol.*, 1998, **118**(2), 107–110.
13 M. E. Karpuzcu, A. J. McCabe and W. A. Arnold, *Environ. Sci.: Processes Impacts*, 2016, **18**(2), 237–245.
14 A. L. Boreen, W. A. Arnold and K. McNeill, *Environ. Sci. Technol.*, 2004, **38**(14), 3933–3940.
15 D. E. Latch, B. L. Stender, J. L. Packer, W. A. Arnold and K. McNeill, *Environ. Sci. Technol.*, 2003, **37**(15), 3342–3350.
16 R. A. Lundeen, C. Chu, M. Sander and K. McNeill, *Environ. Sci. Technol.*, 2016, **50**(16), 8586–8595.
17 V. Nardello, N. Azaroual, I. Cervoise, G. Vermeersch and J.-M. Aubry, *Tetrahedron*, 1996, **52**(6), 2031–2046.
18 W. R. Haag, J. Hoigné, E. Gassman and A. Braun, *Chemosphere*, 1984, **13**(5), 631–640.
19 L. A. A. Sluyterman, *Recl. Trav. Chim. Pays-Bas*, 1961, **80**(9), 989.
20 J. H. Espenson, in *Chemical Kinetics and Reaction Mechanisms*, McGraw-Hill, New York, 1995, pp. 70–100.
21 M. Rougée and R. V. Bensasson, *C. R. Seances Acad. Sci., Ser. 2*, 1986, **302**(20), 1223.
22 A. Jiménez-Banzo, X. Ragàs, P. Kapusta and S. Nonell, *Photochem. Photobiol. Sci.*, 2008, **7**(9), 1003–1010.
23 S. Nonell and C. Flors, in *Singlet Oxygen: Applications in Biosciences and Nanosciences*, 2016, vol. 2, pp. 7–26.
24 P. R. Ogilby, *Chem. Soc. Rev.*, 2010, **39**(8), 3181–3209.
25 H. Wu, Q. Song, G. Ran, X. Lu and B. Xu, *TrAC, Trends Anal. Chem.*, 2011, **30**(1), 133–141.
26 F. Wilkinson, W. P. Helman and A. B. Ross, *J. Phys. Chem. Ref. Data*, 1995, **24**(2), 663–677.
27 S. Nonell and S. E. Braslavsky, *Methods Enzymol.*, 2000, **319**, 37–49.
28 J. Baier, T. Fuß, C. Pöllmann, C. Wiesmann, K. Pindl, R. Engl, D. Baumer, M. Maier, M. Landthaler and W. J. Bäumler, *J. Photochem. Photobiol., B*, 2007, **87**(3), 163–173.
29 A. M. Braun, H. Dahn, E. Gassmann, I. Gerothanassis, L. Jakob, J. Kateva, C. G. Martinez and E. Oliveros, *Photochem. Photobiol.*, 1999, **70**(6), 868–874.
30 P. Di Mascio, M. H. G. Medeiros, H. Sies, S. Bertolotti, S. E. Braslavsky, D. PilóVeloso, B. H. L. N. Sales, E. Magalhães, R. Braz-Filho and E. J. H. Bechara, *J. Photochem. Photobiol., B*, 1997, **38**(2), 169–173.
31 B. Valeur, in *Molecular Fluorescence*, Wiley-VCH Verlag GmbH, 2001, pp. 72–124.
32 H. U. Sverdrup, M. W. Johnson and R. H. Fleming, *The Oceans: their physics, chemistry, and general biology*, Prentice-Hall, New York, 1942.
33 V. Gottfried and S. J. Kimel, *J. Photochem. Photobiol., B*, 1991, **8**(4), 419–430.
34 T. H. Lowry and K. S. Richardson, *Mechanism and Theory in Organic Chemistry*, Harper & Row, New York, 3rd edn, 1987.
35 A. A. Gorman, G. Lovering and M. A. J. Rodgers, *J. Am. Chem. Soc.*, 1979, **101**(11), 3050–3055.
36 A. J. Elliot, D. R. McCracken, G. V. Buxton and N. D. Wood, *J. Chem. Soc., Faraday Trans.*, 1990, **86**(9), 1539–1547.
37 K. Krynicki, C. D. Green and D. W. Sawyer, *Faraday Discuss. Chem. Soc.*, 1978, **66**(0), 199–208.
38 E. Gassmann, *Die Quantenausbeute der Singulettsauerstoff-sensibilisierung in heterogener Phase*, EPFL, 1984.
39 F. E. Scully and J. Hoigné, *Chemosphere*, 1987, **16**(4), 681–694.
40 C. Li and M. Z. Hoffman, *J. Phys. Chem. A*, 2000, **104**(25), 5998–6002.
41 C. Chu, R. A. Lundeen, C. K. Remucal, M. Sander and K. McNeill, *Environ. Sci. Technol.*, 2015, **49**(9), 5511–5519.
42 D. Hillel, *Salinity management for sustainable irrigation: integrating science, environment, and economics; 20842*, The World Bank, 2000, pp. 1–102.
43 R. E. Zeebe and D. Wolf-Gladrow, *CO_2 in Seawater: Equilibrium, Kinetics, Isotopes*, Elsevier, 2001.
44 D. R. Kestel, I. W. Duedall, D. N. Connors and R. M. Pytkowicz, *Assoc. Sci. Limnol. Oceanogr.*, 1967, **12**(1), 176–179.
45 M. E. Q. Pilson, *An introduction to the chemistry of the sea*, Cambridge University Press, Cambridge, 2nd edn, 2013.
46 R. Breslow, *Acc. Chem. Res.*, 1991, **24**(6), 159–164.
47 A. Kumar, *Chem. Rev.*, 2001, **101**(1), 1–20.
48 R. Breslow and T. Guo, *Proc. Natl. Acad. Sci.*, 1990, **87**(1), 167–169.
49 R. D. Shannon, *Acta Crystallogr., Sect. A*, 1976, **32**(5), 751–767.
50 Y. Marcus, *J. Chem. Thermodyn.*, 2012, **48**, 70–74.
51 P. Murasecco, E. Oliveros, A. M. Braun and P. Monnier, *Photobiochem. Photobiophys.*, 1985, **9**(3), 193–201.
52 V. R. Batistela, D. S. Pellosi, F. D. de Souza, W. F. da Costa, S. M. de Oliveira Santin, V. R. de Souza, W. Caetano, H. P. M. de Oliveira, I. S. Scarminio and N. Hioka, *Spectrochim. Acta, Part A*, 2011, **79**(5), 889–897.
53 M. C. Daza, M. Doerr, S. Salzmann, C. M. Marian and W. Thiel, *Phys. Chem. Chem. Phys.*, 2009, **11**(11), 1688–1696.
54 M. Segado and M. Reguero, *Phys. Chem. Chem. Phys.*, 2011, **13**(9), 4138–4148.
55 C. N. Sanramé, R. H. Rossi and G. A. de Argüello, *Photochem. Photobiol.*, 1998, **68**(4), 474–480.
56 R. Schmidt, C. Tanielian, R. Dunsbach and C. Wolff, *J. Photochem. Photobiol., A*, 1994, **79**(1), 11–17.
57 J. P. Tardivo, A. Del Giglio, C. S. de Oliveira, D. S. Gabrielli, H. C. Junqueira, D. B. Tada, D. Severino, R. de Fátima

Turchiello and M. S. Baptista, *Photodiagn. Photodyn. Ther.*, 2005, **2**(3), 175–191.
58 S. C. Núñez and A. S. G., *Photochem. Photobiol. Sci.*, 2014, **13**(3).
59 V. S. Srinivasan, D. Podolski, N. J. Westrick and D. C. Neckers, *J. Am. Chem. Soc.*, 1978, **100**(20), 6513–6515.
60 P. C. Lee and M. A. Rodgers, *Photochem. Photobiol.*, 1987, **45**(1), 79–86.
61 E. Ben-Hur, A. Carmichael, P. Riesz and I. Rosenthal, *Int. J. Radiat. Biol. Relat. Stud. Phys., Chem. Med.*, 1985, **48**(5), 837–846.
62 W. M. Draper and D. G. Crosby, *J. Agric. Food Chem.*, 1983, **31**(4), 734–737.
63 C. E. Diaz-Uribe, M. C. Daza, F. Martínez, E. A. Páez-Mozo, C. L. B. Guedes and E. Di Mauro, *J. Photochem. Photobiol., A*, 2010, **215**(2–3), 172–178.
64 M.-T. Maurette, E. Oliveros, P. P. Infelta, K. Ramsteiner and A. M. Braun, *Helv. Chim. Acta*, 1983, **66**(2), 722–733.
65 C. R. Lambert and I. E. Kochevar, *J. Am. Chem. Soc.*, 1996, **118**(13), 3297–3298.
66 W. W. Wilson and J. R. Heitz, *J. Agric. Food Chem.*, 1984, **32**(3), 615–617.